Registration method for the analysis of mooring chain links degraded by corrosion and wear

Yannick Argouarc'H, Romain Créac'Hcadec

Title

REGISTRATION METHOD FOR THE ANALYSIS OF MOORING CHAIN LINKS DEGRADED BY CORROSION AND WEAR

Author names and affiliations

Y. Argouarc'h[a, *], R. Creac'hcadec[a]

[a] ENSTA Bretagne, UMR CNRS 6027, IRDL, F-29200 Brest, France

* Corresponding Authors

e-mail: yannick.argouarc_h@ensta-bretagne.fr (Y. Argouarc'h)

Abstract

The observation of the three-dimensional geometrical evolution of mooring chain links exposed to the marine environment can be achieved by using 3D scanners. Successive surveys make it possible to precisely identify the location, shapes and quantities of material loss by corrosion or fretting in interlink contact areas. However, the comparison is only possible after an alignment of the obtained scans, because they are not expressed in the same reference marks. The usual point cloud alignment algorithms not being adapted to the expected accuracy, the carried out work implements a new algorithm based on the iterative closest point method (ICP). The developed iterative process of alignment, moves the point cloud corresponding to the aged link onto the new link, after detecting and deleting the points located in the areas of localized material losses (pitting corrosion or wear), and after adding an extra layer on the remaining surfaces, of a value corresponding to the loss of material by a generalized corrosion assumed to be constant. The tests carried out on perfect meshes from CAD constructions show a convergence of the alignment process towards a sufficient precision with regard to the work objectives. Future work can now be considered to test the robustness of the method on meshes from scans of real links or any other mechanical part subject to the same type of physico-chemical aggression that have been in the marine environment.

Keywords:

Mooring chain

Wear

Corrosion

Three-dimensional measurement

Registration

Iterative Closest Point (ICP)

1. Introduction

1.1. Research issue

In the maritime domain, floating structures are anchored to the seabed by mechanical devices usually comprising chains. The design of these marine anchors depends on functional constraints, the characteristics of the implantation sites and the necessary compromises between strength, induced masses and the available reserves of buoyancy. The numerous parameters to be taken into account necessarily influence the interlink movements and the tension supported by the chains. The speed of material loss and wear geometries are therefore variable, and difficult to estimate. As an exemple, Fig. 1(a) illustrates the wear of a chain used to hold a mooring pontoon in a harbor area. This wear, which is groove-shaped and located in the bend of the link, was reproduced experimentally by (Lotfollahi Yaghin and Melchers, 2015) in order to identify the influential parameters and estimate the changes in material loss over time. Fig. 1(b) shows the wear of a chain used for positioning a marine signal buoy in shallow water. The material loss is present over the entire surface of the link and is accentuated in the bends, where there is contact between links.

(a) (b)

Fig. 1. *(a) Interlink wear observed on a mooring pontoon chain in a harbour area. (b) Worn link of a chain used for anchoring a marine signal buoy.*

In the last decade, several studies have identified cases of anchor line failures as well as their origins (D'Souza and Majhi, 2013; Fontaine et al., 2014; Ma et al., 2013). Among these, interlink wear has been identified as one of the parameters requiring further investigation, since, at the contact zone, the reduced diameter contributes to a significant reduction in mechanical strength, which can lead to failure (Gordon et al., 2014). Today, maintenance departments check in situ, once to several times a year, for material losses that are expressed as a percentage of the nominal link diameter. These components must be replaced if this percentage exceeds a maximum value that varies according to use: from 5% in the offshore field (IACS, 2010), up to 40% in the field of maritime signalling (CEREMA, 1997; IALA, 2010). It is noteworthy that this control criterion is not related to the 3D geometry of the material losses, but it is obvious that residual strength is closely related to the type of wear encountered. For example, this control criterion is the same for the two wear patterns described in Fig. 1 as well as for other more atypical material losses, such as the one described in Fig. 2, which is due to a bio-corrosion phenomenon (Eashwar et al., 1992; Murugan et al., 2020). As a result of these considerations, there is some uncertainty about the validity of the commonly used link control criterion, and several further studies have therefore been conducted on this subject, including those carried out by the SCORCH JIP (Seawater COrrosion of Ropes & CHain Joint Industry Project) (Potts et al., 2018).

Fig. 2. *Bio-corroded link after high pressure cleaning*

In order to further improve the knowledge of the relationships between residual strength of mooring chains and 3D wear geometries, a method is here provided that will allow to precisely describe the typologies of material loss encountered - wear or corrosion - as well as their spatial distribution on the link, and the quantities of material loss. This work can be envisaged with the use of 3D scanners, which enable contact-free measurements to be taken, often with the use of laser or by projecting structured light. This technology provide point clouds, or after computer

processing, provide files, for example STL (Standard Tesselation Language), containing more information such as the surface mesh (see Fig. 3), the associated normals or possibly colours.

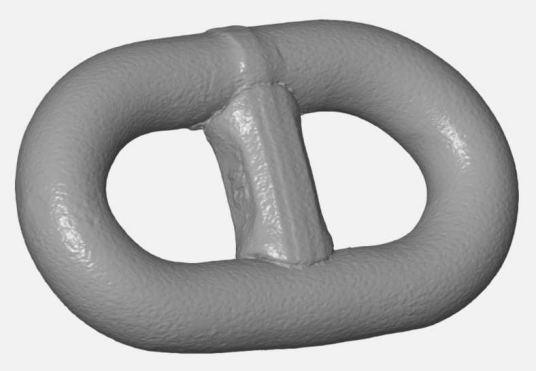

Fig. 3. *Scan of stud link.*

In order to identify the material losses of a link, it is necessary to compare its 3D geometries, before and after being in the marine environment. This comparison is only possible if the geometries are superimposed, i.e. written in the same reference frame. For example, this superposition can be achieved by using a shape recognition algorithm that aligns each scan to a theoretical link skeleton (Emmanuel Fontaine et al., 2014). However, this process depends on the theoretical shape of the skeleton used, which does not take into account neither manufacturing tolerances nor the presence of material losses due to corrosion or wear. It is therefore proposed here to directly align the 3D geometries of the links by a new method whose performance will be evaluated, without using a theoretical link skeleton. This alignment operation is termed "registration", a mathematical process that allows the writing of data in the same coordinate system, while minimising alignment error. An early publication on this subject termed this problem "*Orthogonal proscrustes*" (Hurley and Cattell, 1962). Today, most registration methods are based on an algorithm called "Iterative Closest Point", which was proposed by (Besl and McKay, 1992) and which identifies the rigid-body motion allowing the superposition of data. The numerous applications of this method to the different specificities encountered have led to a significant increase in publications in this field since the 2000s. Several bibliographical studies list these applications and sometimes propose performance comparisons (Bellekens et al., 2015; Bowyer et al., 2006; Fontana et al., 2020; Pomerleau et al., 2015). In our case, the goal is the accurate superposition of two scans describing a link whose geometry has varied due to fretting and corrosion. It is therefore proposed in this publication to validate a robust and automatic method, derived from the Iterative Closest Point (ICP) algorithm to achieve the defined goal.

1.2. Means and methods for acquiring 3D images

The data that will be used in this study are of two types. The first is from CAD objects whose parameterised construction enables exact geometries to be defined. The other is from scans of real links, either naturally worn in the marine environment, or new. As the chain links cannot be dismantled and monitoring the wear over time imposes a non-destructive measurement method, the sampling of a single link to obtain these data is prohibited. The links are therefore scanned in the presence of the two adjacent links, but also in the presence of a holding device. Consequently, it is necessary to perform several successive scans (see Fig. 4) from different perspectives in order to acquire the entire geometry of the part. The data are then processed on the 3D scanner manufacturer's software (*Artec studio professional 15*, 2020) and exported as STL files. These files describe the surface of the parts by means of meshes composed of facets whose vertices are defined in a Cartesian reference frame.

Fig. 4. *Scan of stud link without processing, with the holding support and the adjacent links.*

The scans of the links are carried out with a calibrated hand-held device of the Artec Space Spider type with a measurement error, as claimed by the manufacturer, of less than 0.05 mm (error control carried out from measurement tests on calibrated spheres). The resolution of the device, which corresponds to the minimum size of the edges of the mesh, is equal to 0.15 mm. Subsequently, in order to acquire maximum information on the contact wear between links, it was decided to choose values close to the minimum resolution of the device, despite the negative consequences in terms of the storage capacity required and the computation time induced. The algorithm proposed in this publication was developed in Python 3.6, in the Anaconda environment. The library used to facilitate the use of the STL files is Trimesh (Dawson-Haggerty, 2019). All computations were performed on a Dell Latitude 5590-16, i5-8350U computer with 16 GB of RAM.

1.3. Designation and coordinate system

To name the links, three defined parameters from the new geometries are usually used: the diameter d, the length coefficient C_g and the width coefficient C_b. The length coefficient multiplied by the diameter is equal to the length L_g of the link, the width coefficient multiplied by the diameter is equal to the width L_b of the link (see Fig. 5(a)). For example, a stud link named 40-6-3.4 has a diameter of 40 mm, a length of 240 mm and a width of 136 mm, before aging.

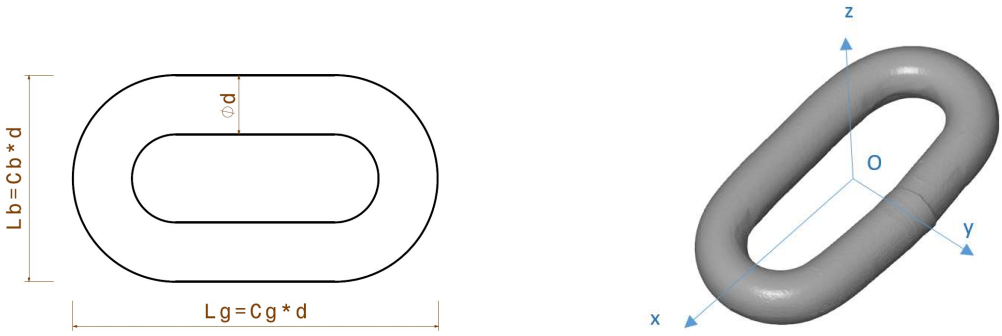

(a) (b)

Fig. 5. *(a) Link size. (b) Reference mark of the link.*

The local orthonormal reference frame $R(O, \vec{x}, \vec{y}, \vec{z})$ associated with the links is defined in Fig. 5(b). The origin is located at the geometric center of the link. The direction of the $\vec{x}$ axis is along the longest length of the link and is oriented toward the seafloor for the actual links. The direction of the $\vec{y}$ axis is laterally toward the weld. The $\vec{z}$ axis is the complementary axis.

2. Distance measurement

As the ultimate objective of this work is to identify losses of material, it is necessary to compare the geometries of a link, in two different states, based on distance calculations. Moreover, the registration algorithm that will be described in this publication is based on the minimisation of a criterion that too is built from the distances between the three-dimensional meshes of the two links analysed. The ability to accurately measure a distance between two meshes is therefore central to the general process of losses of material identification. It is therefore essential here to provide a detailed description of the two distance calculation methods that will be used later.

2.1. Point-to-point distance

2.1.1. Point-to-point distance description

Let S_p be a real surface supporting a mesh M_p whose nodes form a point cloud Pc_p composed of n_p points P_j. Let Q_i be any point in space, and Q_i and P_j have coordinates $\vec{q}_i$ et $\vec{p}_j$ respectively in the Cartesian reference frame $R_0(O, \vec{x}_0, \vec{y}_0, \vec{z}_0)$.

The distance from Q_i to P_j, denoted $d(Q_i, P_j)$, is the Euclidian distance such that:

$$d(Q_i, P_i) = \left\| \vec{p}_j - \vec{q}_i \right\| \quad (1)$$

The distance from Q_i to the surface S_p, denoted $d(Q_i, S_p)$, is approximated in this first method by the distance from Q_i to the point cloud Pc_p, denoted $d(Q_i, Pc_p)$. This distance is defined as the distance from Q_i to its nearest point, within Pc_p:

$$d(Q_i, S_p) \cong d(Q_i, Pc_p) = min_{i\in(1,n_p)}[d(Q_i, P_i)] \quad (2)$$

Let $P_k(Q_i)$ be the k^{th} point closest to Q_i within Pc_p, such that the distance from Q_i to the point cloud Pc_p can be written :

$$d(Q_i, Pc_p) = d(Q_i, P_1(Q_i)) \quad (3)$$

The distances obtained are signed as a function of the normal $\vec{n}\left(P_1(Q_i)\right)$ to the surface S_p , at the closest point $P_1(Q_i)$. This normal has an outwardly direction from the material, and the distances are considered positive if $(\overrightarrow{p_1}(Q_i) - \vec{q}_i).\vec{n}\left(P_1(Q_i)\right) \geq 0$. The normal $\vec{n}\left(P_1(Q_i)\right)$ is obtained relatively simply in this first distance calculation method, by the normalised sum of the normals of the facets adjacent to the point $P_1(Q_i)$.

Since n_p, the number of points of the mesh M_p, is often high, the computation time $O(n_p)$ associated with identifying the closest point $P_1(Q_i)$ is significant. It is therefore preferable to partition the space in order to reduce this computation time. It is proposed here to use a k-d tree (Maneewongvatana and Mount, 1999), which iteratively

partitions the parent space, for example, by dividing it equally. After constructing a single tree in the algorithm, for a computation time $O(n_p \log n_p)$, the search time for the nearest point in this tree drops to around $O(\log n_p)$. In addition to the computation time benefit, k-d tree implementations, for example ("Scipy spatial KDTree," 2011), make it easy to identify the first k nearest points $P_k(Q_i)$, constrained, if necessary, by a maximum distance to the point Q_i which is not to be exceeded.

2.1.2. Point-to-point distance tests

Since the point cloud Pc_p is a real representation of the real surface S_p, it is necessary to question the error made by computing $d(Q_i, Pc_p)$ instead of $d(Q_i, S_p)$. In the following example, we consider a spherical surface S_p of radius R positioned at O, the center of the Cartesian reference frame. This sphere is the support for a triangular mesh M_p whose edge length does not exceed the value b_s. A number n_q of points Q_i is randomly generated and the distances $d(Q_i, Pc_p)$ are computed using the point-to-point method and compared to the exact distances $d(Q_i, S_p)$. The fixed values are as follows: $R = 10$ mm, $b_s = 0.207$ mm and $n_q = 5000$.

Fig. 6 plots the absolute value of the error made as a function of $\|\vec{q}_i\|$, the distance from origin O to the point Q_i. This figure shows that the closer the Q_i points are to the sphere, the larger the error is. The processing time that was required to calculate these n_q distances is equal to 15.6 s.

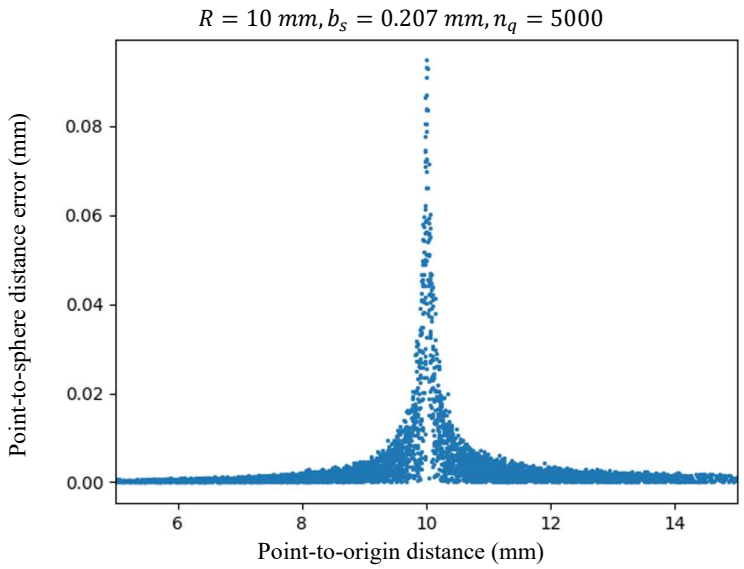

Fig. 6. *Errors concerning distances computed between random points and a sphere. The distances are estimated using the point-to-point method.*

A simple reasoning illustrated by Fig. 7 shows that points Q_i, close to the real surface S_p, necessarily induce a significant error. The maximum error, $b_s/2$, is reached in the unfavorable case where the point Q_i is located in the middle of the longest edge of the mesh.

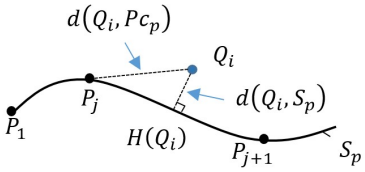

Fig. 7. *Approximation in a point-to-point distance calculation. Here, $H(Q_i)$ is the closest point to Q_i on S_p.*

Consequently, the distance calculation method presented here can be adapted if the distances to be measured are large with respect to b_s, the maximum length of the edges of the mesh. As this value is close to 0.15 mm in our work and as the expected accuracy in our calculations is much lower than the accuracy of the measuring device (0.05 mm), a more precise method of calculating distance has been developed.

2.2. Point-to-curve distance

2.2.1. Point-to-curve distance calculation

In order to improve the accuracy of the distance calculation, it is proposed to locally approximate the surface S_p by means of a polynomial smoothing curve $C_p(Q_i)$, constructed from the first m closest points to Q_i. The distance of the point Q_i to the surface S_p is thus calculated, using this method, by means of the distance from Q_i to the nearest point $H(Q_i)$ forming part of the curve $C_p(Q_i)$.

$$d(Q_i, S_p) \cong d(Q_i, C_p(Q_i)) = min_{P \in C_p(Q_i)}[d(Q_i, P)] = d(Q_i, H(Q_i)) \quad (4)$$

The smoothing operation is performed in a new reference frame $R_1(O, \vec{x}_1, \vec{y}_1, \vec{z}_1)$ such that the normal to the first nearest point is carried by $\vec{z}_1$. In this new reference frame R_1, a point P with coordinates (x, y, z) forms part of the smoothing curve $C_p(Q_i)$ if its coordinates verify equation (5).

$$z = f_p(x, y) = c_9x^3 + c_8y^3 + c_7x^2y + c_6xy^2 + c_5x^2 + c_4y^2 + c_3xy + c_2x + c_1y + c_0 \quad (5)$$

In the plane $(O, \vec{x}_1, \vec{y}_1)$, the area that is defined by the smallest oriented rectangle containing the projections of the m nearest points is called the area of interest $Iz(Q_i)$ of the point Q_i. The maximum and minimum z coordinates of the set of points $P_k(Q_i)$ are respectively z_m and z_M. In order to limit the search area of the point $H(Q_i)$, a search area $Rz(Q_i)$ (see Fig. 8) smaller than $Iz(Q_i)$ has been defined. Due to the definition of the reference frame R_1, it is notable that the direction of the line $\left(Q_i H(Q_i)\right)$ is close to $\vec{z}_1$. Therefore, the search area $Rz(Q_i)$ of point Q_i is centred on the projection of point Q_i in the plane $(O, \vec{x}_1, \vec{y}_1)$. Assuming that the projection of $H(Q_i)$ in the plane $(O, \vec{x}_1, \vec{y}_1)$ is no further away than that of the second closest point $P_2(Q_i)$, the geometry of the search area can be defined by an oriented square whose side $b(Q_i)$ is given by equation (6).

$$b(Q_i) = 2 \times \max \{abs\,[(\overrightarrow{p_2}(Q_i) - \vec{q}_i)\,.\vec{x}_1], abs[(\overrightarrow{p_2}(Q_i) - \vec{q}_i)\,.\vec{y}_1]\} \tag{6}$$

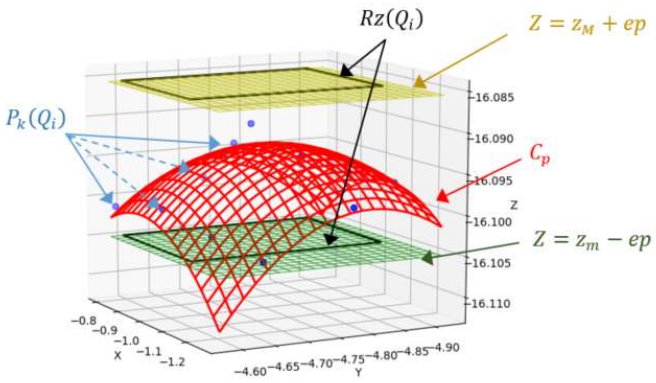

Fig. 8. *Illustrative diagram of the definition of smoothing.*

It is proposed, in this method of distance calculation, to successively increment the degree of the polynomial until the smoothing is considered correct. The defined smoothing is thus planar, otherwise quadric, otherwise cubic. At each polynomial degree, the quantity m of nearest points used must simply be greater than or equal to the number of parameters sought. It was considered preferable to keep this value m fixed whatever the degree of the polynomial so that the area of interest $Iz(Q_i)$ remains relatively constant whatever Q_i. A value equal to 12 was considered sufficient during our calculations. Once parameters c_i are identified, the smoothing is considered valid if it verifies three conditions.

First condition: at each of the m closest points $P_k(Q_i)$, the absolute value of the error remains less than e_p(mm), an imposed value (e.g. 0.005 mm).

$$\left|z_{P_k(Q_i)} - f_p\left(x_{P_k(Q_i)}, y_{P_k(Q_i)}\right)\right| \leq e_p \,, \forall k \in (1, m) \tag{7}$$

Second condition: in the search area $Rz(Q_i)$, the z−coordinates of the curve C_p must remain bounded between $z_m - e_p$ and $z_M + e_p$

$$z_m - e_p \leq \left|f_p(x, y)\right| \leq z_M + e_p \,, \forall (x, y) \in Rz(Q_i) \tag{8}$$

Third condition: no point $P_k(Q_i)$ among the points closest to Q_i is located on a border of the mesh M_p.

The first condition reflects the need for $C_p(Q_i)$ to pass as close as possible to the points $P_k(Q_i)$, material points extracted from the mesh of the surface S_p. The second condition is related to the possibility that the points $P_k(Q_i)$ are partially aligned, which leads to inappropriate curves $C_p(Q_i)$, with strong undulations (see Fig. 9). This phenomenon is often observed for meshes obtained from CAD constructions. The third condition prohibits distance measurements on mesh borders.

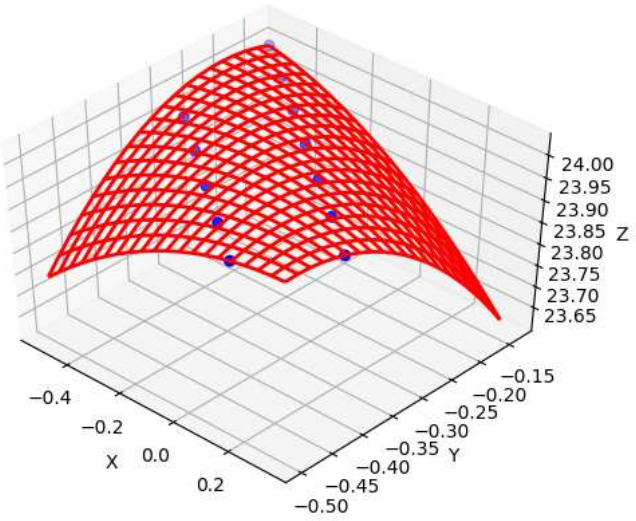

Fig. 9. *Cp curve on partially aligned points, resulting in inappropriate smoothing*

If one of the conditions for the validity of $C_p(Q_i)$ is not verified, the distance calculation method described here does not return any result for the point Q_i concerned. If all the conditions are validated, the distance of Q_i to the real surface S_p is then approximated by the minimal distance of Q_i to the analytical curve $C_p(Q_i)$. The search for

this minimum value is performed by sequential quadratic programming (Kraft, 1988) on the search area $Rz(Q_i)$. In other terms:

$$d(Q_i, S_p) \cong d(Q_i, C_p(Q_i)) = d(Q_i, H(Q_i)) = min_{(x,y)\in Rz(Q_i)}\{d(Q_i, P[x, y, f_p(x, y)])\} \quad (9)$$

The distances obtained are signed as a function of the normal $\vec{n}\,(H(Q_i))$, which is external to the surface $C_p(Q_i)$ and located at the nearest point $H(Q_i)$. This normal is computed, in a postprocessor, by means of a derivation of the function f_p. Ultimately, this distance calculation method allows us to obtain :

- the distance $d(Q_i, S_p)$,
- the nearest point $H(Q_i)$ on $C_p(Q_i)$,
- a set of points Q_i on the basis of which the smoothing is rejected,
- in a postprocessor, by means of a derivation of f_p, the computation at the point $H(Q_i)$ of the normal to the curve $C_p(Q_i)$, denoted $\vec{n}\,(H(Q_i))$.

2.2.2. Point-to-curve distance tests

2.2.2.1. Application on sphere

It is proposed here to take the example of the sphere from paragraph 2.1.2 and to carry out the distance error calculations of the point-to-curve method for two calculation accuracies: e_p : 0.005 mm and 0.002 mm. The processing times are measured and compared to those of the point-to-point method by estimating a percentage increase. The results are summarised in Table 1.

Table 1 *– Calculation error concerning sphere*

	e_p (mm)	Quantity of planar smoothing	Quantity of quadric smoothing	Quantity of cubic smoothing	Maximum error (mm)	Calculation time (s)	Increase of calculation time (%)
Case 1	0.005	5000	0	0	0.0037	26.01	67
Case 2	0.002	0	5000	0	4.7e-7	38.64	147

The results show that for an expected accuracy of 0.005 mm, a planar smoothing is sufficient. For the value of e_p of 0.002 mm, a quadric smoothing is systematically selected and the calculated error is very close to zero. Concerning the calculation times, they are much higher than those obtained for the point-to-point method. It is also possible to observe that these errors no longer depend on the proximity of Q_i to the sphere (see Fig. 10), which was the goal.

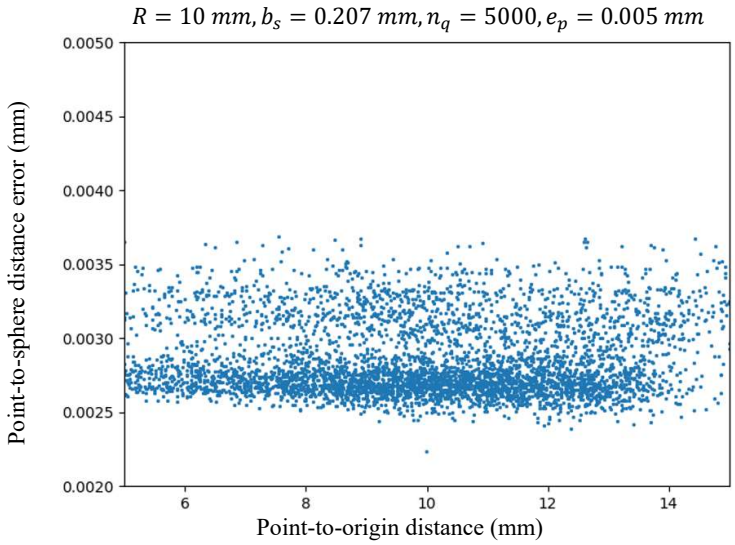

***Fig. 10**. Error concerning distances calculated between random points and a sphere. Distances are estimated using the point-to-curve method.*

2.2.2.2. Applications to chain links

In this example, several point-to-curve distance calculations are processed from six different studless link geometries, superimposed in pairs, in the same reference frame. For each case, 5000 distance calculations are performed, the e_p value is taken to be 0.005 mm, then 0.002 mm. Links Li_0, Li_1, Li_2, Li_3 are links obtained by means of CAD construction. Links Li_1, Li_2, Li_3 are derived from link Li_0 (see Fig. 11(a)) after a material thickness reduction t_{hk} of 0.05 mm, 0.5 mm and 5 mm, respectively. The expected distances for the distance calculations then correspond to these material thickness reductions. The link Li_4 (see Fig. 11(b)) is from the scan of a new link with a relatively smooth surface. Link Li_5 (see Fig. 11(c)) is from a worn link scan with a rough surface, highly altered by bio-corrosion. Since these last two links are superimposed on themselves, the expected distances are zero. The characteristics of the six links are shown in Table 2. The results of the distance calculations are summarised in Table 3.

Table 2 *– Characteristics of the links*

Links	b_s (mm)	t_{hk} (mm)	n_p	File size (Mo)
Li_0	0.28	0	1 124 304	110
Li_1	0.28	0.05	1 119 540	110
Li_2	0.28	0.5	1 078 896	105
Li_3	0.28	5	703 420	69
Li_4	0.29	0	1 003 308	98
Li_5	0.34	0	1 048 985	102

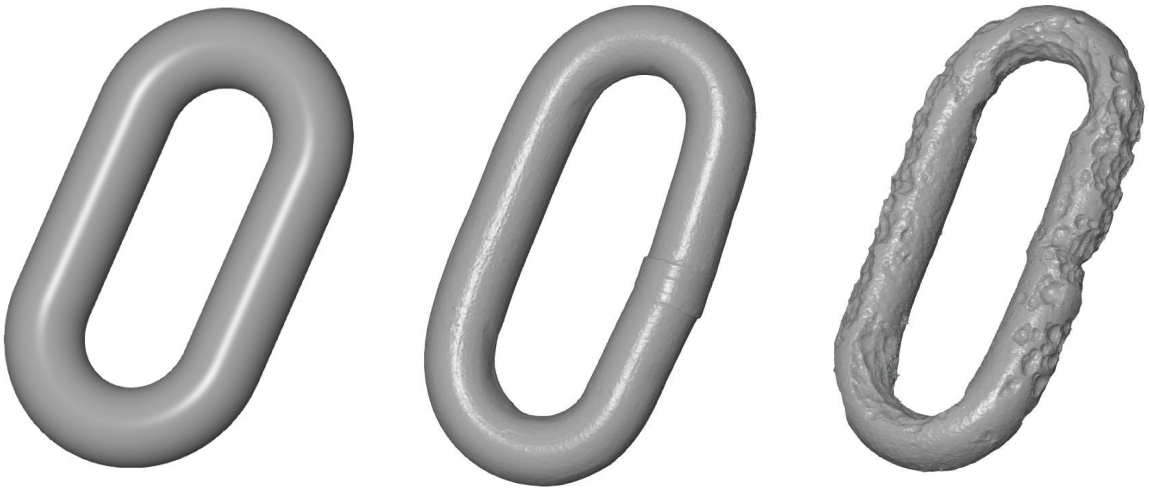

(a) (b) (c)

Fig. 11*. (a) Link* Li_0*, CAD construction, designation 30-6-3.4. (b) Link* Li_4*, scan of new real link, designation 20-7-3.4. (c) Link* Li_5*, scan of an aged real link, designation 20-7-3.4.*

Table 3 *– Point-to-curve distance results*

Links		e_p (mm)	Quantity of planar smoothing	Quantity of quadric smoothing	Quantity of cubic smoothing	Number of rejected points	Maximum error (mm)
Li_0	Li_1	0.005	5000	0	0	0	0.0019
Li_0	Li_1	0.002	3133	1867	0	0	0.0017
Li_0	Li_2	0.005	5000	0	0	0	0.0019
Li_0	Li_2	0.002	3761	1239	0	0	0.0019

Li_0	Li_3	0.005	5000	0	0	0	0.0022
Li_0	Li_3	0.002	3900	1100	0	0	0.0019
Li_4	Li_4	0.005	2827	1722	301	150	0.0050
Li_4	Li_4	0.002	335	2296	1258	1111	0.0020
Li_5	Li_5	0.005	450	1939	1597	1014	0.0050
Li_5	Li_5	0.002	17	560	1771	2652	0.0020

These results show that the errors are all smaller than the set e_p value. Furthermore, as the expected accuracy increases, the degree of the polynomial tends to increase and the number of rejected points also increases, reaching as high as 53% in the case of the highly worn Li_5 link.

2.3. Discussion of distance calculation methods

The first method of point-to-point calculation estimates the distance of a point Q_i to a surface S_p, by means of the distance between this point Q_i and a sample of points forming part of the surface S_p. This method enables results to be obtained quickly, but the relative error becomes significant when Q_i is close to S_p. The second computational method estimates the distance of a point Q_i to a surface S_p, by means of the distance between this point Q_i and a curve passing, at best, through the m closest points in Pc_p. This method, which induces a much longer computation time, allows a measurement quality that does not depend on the distance of Q_i to the surface S_p, and the error committed remains lower than the fixed e_p value. If the smoothing associated with a point Q_i does not verify certain criteria, the calculation does not return a result and the point is said to be rejected. The lower the parameter e_p, the more difficult the smoothing becomes and the higher the number of rejected points Q_i. Therefore, for each type of scanned surface, a compromise must be found between the desired accuracy, the calculation time and the number of rejected points.

The specific registration methods that will be presented in the following chapters require the use of the two types of distance calculations described here. The first one for fast calculations without a need for precision, the second one in the opposite cases.

3. Registration for corroded link

3.1. Focus of the problem

Let two surfaces S_p and S_q be exact observations of the same surface S. The surfaces S_p and S_q are the supports for two meshes M_p and M_q whose nodes form point clouds Pc_p and Pc_q, composed of n_p and n_q points, P_j and Q_i. The objective of a registration between S_p and S_q is to find the rigid transformation $\mathcal{T}$ such that the distances between S_p and $\mathcal{T}(S_q)$ are zero. This objective can be translated by condition (10), or discretely on the point cloud Pc_q, by condition (11).

$$\forall\, Q \in S_q, d\left(S_p, \mathcal{T}(\mathrm{Q})\right) = 0 \tag{10}$$

$$\forall\, Q_i \in Pc_q, d\left(S_p, \mathcal{T}(\mathrm{Q}_i)\right) = 0 \tag{11}$$

In a general case, the two surfaces S_p and S_q are imperfect observations of the same surface S due to, among other things, the inaccuracy of the acquisition device. Identifying the transformation $\mathcal{T}$ that best aligns the two surfaces S_p and S_q can then be achieved by minimising an objective function $g(S_p, Pc_q)$, as defined by expression (12).

$$g(S_p, Pc_q) = \sum_{i=1}^{n_q} \left[d\left(S_p, \mathcal{T}(\mathrm{Q}_i)\right)\right]^2, \mathrm{Q}_i \in Pc_q \tag{12}$$

We subsequently define the target point Pt_i, as the closest point on S_p, to the image of Q_i by means of the transformation $\mathcal{T}$. Expressing $g(S_p, Pc_q)$ as a function of Pt_i and considering only a sample Ec_q of N points of Pc_q, we obtain the new objective fonction (13).

$$g(S_p, Ec_q) = \sum_{i=1}^{N} \left[d\left(Pt_i, \mathcal{T}(\mathrm{Q}_i)\right)\right]^2, \mathrm{Q}_i \in Ec_q \tag{13}$$

Note that the closest points $\mathrm{H}(\mathrm{Q}_i)$ of Q_i on S_p, are different from the target points Pt_i (see Fig. 12), but the more aligned the surfaces S_p and S_q are, the more these points tend to merge.

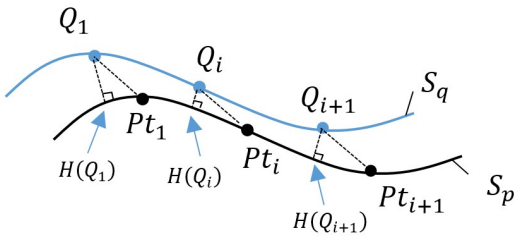

Fig. 12. *Target points and nearest points*

If the points P_j et Q_i. are represented by homogeneous coordinates, it is possible to define the spatial transformation $\mathcal{T}$ using the matrix T described by expression (14) in order to easily move the point clouds Pc_p and Pc_q through space.

$$T = \begin{bmatrix} & R_{3\times3} & & t_{3\times1} \\ 0 & 0 & 0 & 1 \end{bmatrix} \tag{14}$$

The matrix T is composed of a rotation matrix R of $SO(3)$ that can be constructed from three angular parameters (e.g. Euler angles), and a translation vector $\vec{t}$ that is defined by three length parameters. Thus, six parameters are needed to define T. The objective function $g(S_p, Ec_q)$ can therefore be translated into the following equation (15) :

$$g(S_p, Ec_q) = \sum_{i=1}^{N} \left[d(\overrightarrow{\mathrm{pt}_i}, T\vec{q}_i)\right]^2 = \sum_{i=1}^{N} \left\|\overrightarrow{\mathrm{pt}_i} - T\vec{q}_i\right\|^2, \mathrm{Q}_i \in Ec_q \tag{15}$$

Minimising $g(S_p, Ec_q)$ identifies the spatial transformation $\mathcal{T}$ that best overlays S_q onto S_p. The search for this minimum is complex, and highly non-linear. After this superposition, the meshes are said to be "aligned" or "registered".

3.2. Iterative Closest Point (ICP)

3.2.1. General description of the ICP method and implementation

3.2.1.1. General description

The most common method of identifying the desired $\mathcal{T}$ transformation is the Iterative Closest Point (ICP) method (Besl and McKay, 1992). This method iteratively brings S_q towards S_p. At each iteration k, the objective is to find the transformation $\mathcal{T}_k$ that minimises the objective function g_k defined by expression (16). The points $\mathrm{Q}_{i,k-1}$ are the points of $Ec_{q,k-1}$ displaced, in the previous iteration, by the identified transformation $\mathcal{T}_{k-1}$.

$$g_k(S_p, Ec_{q,k-1}) = \sum_{i=1}^{N} \left[d\left(\mathrm{Pt}_i, \mathcal{T}_k(\mathrm{Q}_{i,k-1})\right)\right]^2, \mathrm{Q}_{i,k-1} \in Ec_{q,k-1} \tag{16}$$

An initial phase of surface pre-positioning allows us to assume that the target points Pt_i are close to $\mathrm{H}(\mathrm{Q}_{i,k-1})$, the points closest to $\mathrm{Q}_{i,k-1}$ on S_p. The points Pt_i are then replaced in (16) by the points $\mathrm{H}(\mathrm{Q}_{i,k-1})$ easily determined by the distance calculation methods developed in Chapter 2. Expression (16) can then be simplified by expression (17), which has only the six unknowns of the transformation matrix T_k.

$$g_k(S_p, Ec_{q,k-1}) = \sum_{i=1}^{N} \left[d\left(\mathrm{H}(\mathrm{Q}_{i,k-1}), \mathcal{T}_k(\mathrm{Q}_{i,k-1})\right)\right]^2, \mathrm{Q}_{i,k-1} \in Ec_{q,k-1} \tag{17}$$

Once T_k has been identified, the sample of points $Ec_{q,k-1}$ is moved by means of the T_k transformation. The iterations continue until a convergence criterion is reached. Additional elements to specify the ICP method are described in a non-exhaustive manner below.

Sample: the point sample Ec_q can be chosen randomly in Pc_q but, more optimally, it is also possible to choose points uniformly distributed over the surface S_q (Turk and Levoy, 1994).

Objective fonction: many variants of the objective function g_k exist in the literature. Many of them propose different choices of points that best approximate the target points Pt_i. For example, the nearest point on Pc_p (Besl and McKay, 1992) or nearest point on a plane tangent to S_p (see Fig. 13), constructed at the first nearest point on Pc_p (Chen and Medioni, 1992).

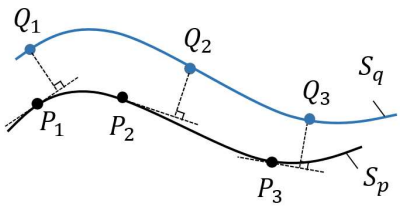

Fig. 13. *Distance point - plan*

Resolution: each transformation matrix T_k can be obtained by minimising g_k using a gradient descent method or, more robustly, an SVD (singular-value decomposition) method (Arun et al., 1987; Sorkine-Hornung and Rabinovich, 2017). At the end of the process, the transformation matrix T sought is the product of all transformation matrices obtained at each iteration:

$$T = \prod_k T_k \tag{18}$$

Convergence criterion: it can be, for example, a maximum number of iterations, a minimum standard deviation, or a minimum threshold of variation of the objective function as proposed by the inequation (19):

$$|g_k - g_{k-1}| \leq \varepsilon_g \; with \; (\varepsilon_g > 0) \tag{19}$$

Initialisation: to initiate the calculation, the meshes M_p and M_q must be close to each other. Otherwise, the computation time risks being significantly increased or the convergence of the algorithm may not even be achieved. This initial positioning operation can be performed by aligning the principal components (PCA) of the covariance matrix of each point cloud (Yambor et al., 2002) or aligning the smallest parallelepipeds containing the point clouds.

General algorithm: the algorithm of the ICP method is described as follows.

a)- Approximate initial alignment of M_q onto M_p.

b)- Selection of a sample Ec_q of N points Q_i in Pc_q

Start of iteration k

c)- For each $Q_{i,k-1}$ in $Ec_{q,k-1}$ estimation of the target point Pt_i on S_p.

d)- Identification of the transformation T_k by minimising g_k.

e)- Displacement of $Ec_{q,k-1}$ by means of the transformation T_k.

f)- Computation of the convergence criterion.

Loop-back if criterion not verified.

g)- Computation of the total transformation matrix T.

h)- Displacement of the mesh M_q by the transformation T.

3.2.1.2. Implementation of the ICP method

In order to perform registration tests on chain links, an implementation of the ICP method is used. This includes the following specificities:

Sample: the N points of the sample Ec_q are selected randomly. Following many tests, the optimal number of points needed to express the objective function is set to 400. During the initial selection of the sample, however, this value must be increased to take into account the proportion of rejected points during the point-to-curve distance calculations. This proportion of rejected points is initially identified by performing, for each mesh M_p and M_q, a point-to-curve distance calculation of the mesh concerned, onto itself (distances expected to be zero). These initial tests also allow us to identify, for each sample point Ec_q, the normals calculated on the smoothing curves.

Objective function: the objective function g_k is defined by equation (17). The identification of the corresponding points $\mathrm{H}(\mathrm{Q}_{i,k-1})$ is performed during the first fifteen iterations by the point-to-point method to induce a fast approach phase. The point-to-curve method, which is slower, is then used for a precise registration. The accuracy e_p is then fixed at 0.005 mm.

Resolution: the transformation matrices T_k are obtained using the SVD (singular-value decomposition) method.

Convergence criterion: the iterative process continues for as long as the number of iterations does not exceed 120 and the standard deviation of the distances between the meshes is greater than 0.003 mm.

Initialisation: the initial position is set by aligning the smallest parallelepipeds containing the point clouds. Because of the symmetries of the geometry of the links, an additional visual check is necessary to ensure that the

orientations of the local reference frame of the links correspond. This initialisation phase can be omitted if the links are initially close enough, which will be the case in all the tests performed in this article.

3.2.2. ICP method tests

3.2.2.1. Application to identical links

Three uncorroded links are used to test the implementation of the ICP method. These are the links Li_0, Li_4 and Li_5 described in section 2.2.2. For each link, a copy is moved through space by means of a geometric transformation. Two cases are studied $(R_y, T_x) = (3°, 2\ mm)$ and $(R_y, T_x) = (6°, 5\ mm)$. The objective of the registration is to realign the copy onto the initial link. At the end of the process, the distances between links are expected to be zero. At each iteration, the calculated point-to-curve distances are used to compute the mean and standard deviation of the distances. These values can be seen in Fig. 14 and Fig. 15 for the transformation $(R_y, T_x) = (3°, 2\ mm)$. Additionally, the number of iterations as well as the computation time are recorded at the end of the process. The final results are summarised in Table 4.

Table 4 *– ICP applied to identical links*

Fixed link	Moved link	R_y (degree)	T_x (mm)	Mean (mm)	Standard deviation (mm)	Maximum error (mm)	Number of iterations	Calculation time (s)
Li_0	Li_0	3	2	-0.0011	0.0004	0.0019	11	46
Li_0	Li_0	6	5	-0.0011	0.0030	0.0084	39	279
Li_4	Li_4	3	2	-0.0000	0.0030	0.0031	48	339
Li_4	Li_4	6	5	-0.0003	0.0028	0.0097	63	475
Li_5	Li_5	3	2	-0.0001	0.0030	0.0084	36	271
Li_5	Li_5	6	5	-0.0000	0.0029	0.0077	41	332

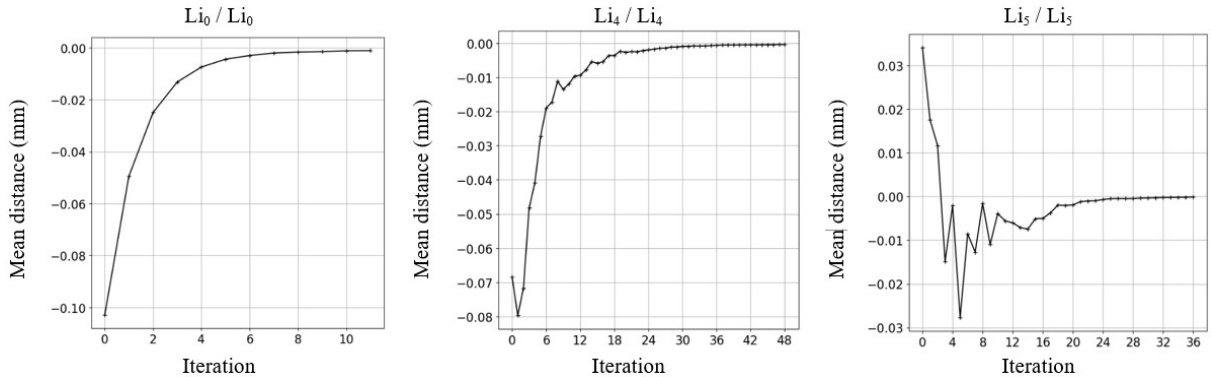

Fig. 14. *ICP method applied to uncorroded links. Mean distance for Li_0, Li_4 and Li_5 with R_y=3° and T_x=2 mm.*

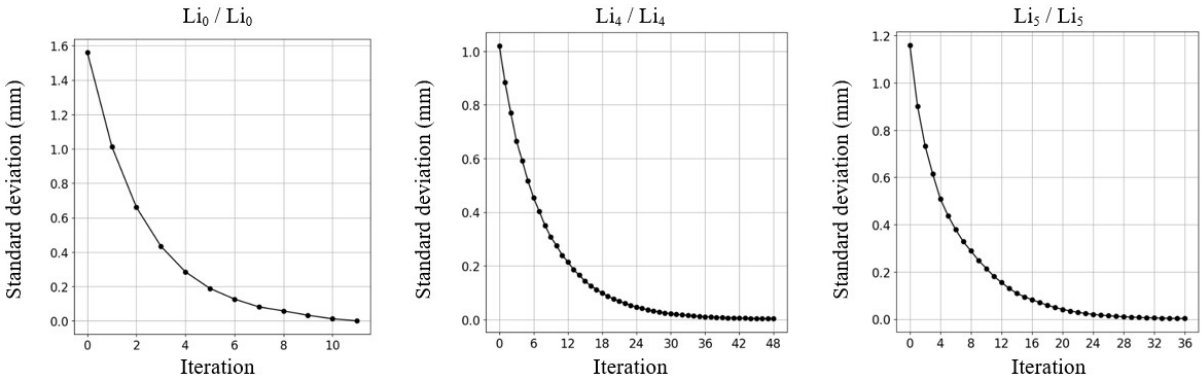

Fig. 15. ICP method applied to uncorroded links. Standard deviation of distances for Li_0, Li_4 and Li_5 with R_y=3° and T_x=2 mm.

3.2.2.2. Application to corroded links

The major assumption that allows the use of the ICP method for corroded links is a generalised corrosion assumption: at any point on the link the material loss is identical and is equal to t_{hk} mm. The process of minimising g_k can therefore also be considered in order to superimpose these links. The implementation of the ICP method for corroded links is tested on the basis of CAD links only because it is difficult to obtain standard links that can be used as reference. These are the Li_1, Li_2 and Li_3 described in chapter2.2.2. Each of these links is moved through space by means of a geometric transformation. The goal of registration is to realign these links to Li_0, the initial CAD link. At the end of the process, the expected distances between links are equal to t_{hk}. The results are parametised and analysed in the same way as for the previous tests. The results of these calculations are summarised in Table 5, in Fig. 16 and Fig. 17.

***Table 5** - ICP applied to corroded links*

Fixed link	Moved link	R_y (degree)	T_x (mm)	Mean (mm)	Standard deviation (mm)	Maximum error (mm)	Number of iterations	Calculation time (s)
Li_0	Li_1	3	2	0.0477	0.0074	0.0166	80	692
Li_0	Li_1	6	5	0.0476	0.0079	0.0192	80	669
Li_0	Li_2	3	2	0.4878	0.0742	0.1452	80	660
Li_0	Li_2	6	5	0.4859	0.0802	0.1891	80	654
Li_0	Li_3	3	2	4.8332	1.0462	2.2125	80	804
Li_0	Li_3	6	5	4.8124	1.0940	2.2577	80	774

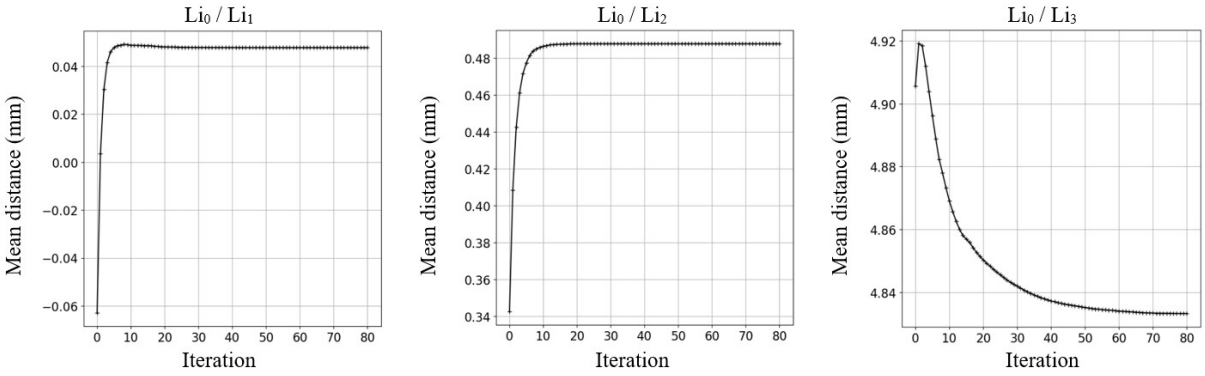

Fig. 16. ICP method applied to corroded links. Mean distance for Li_1, Li_2 and Li_3 with R_y=3° and T_x=2 mm.

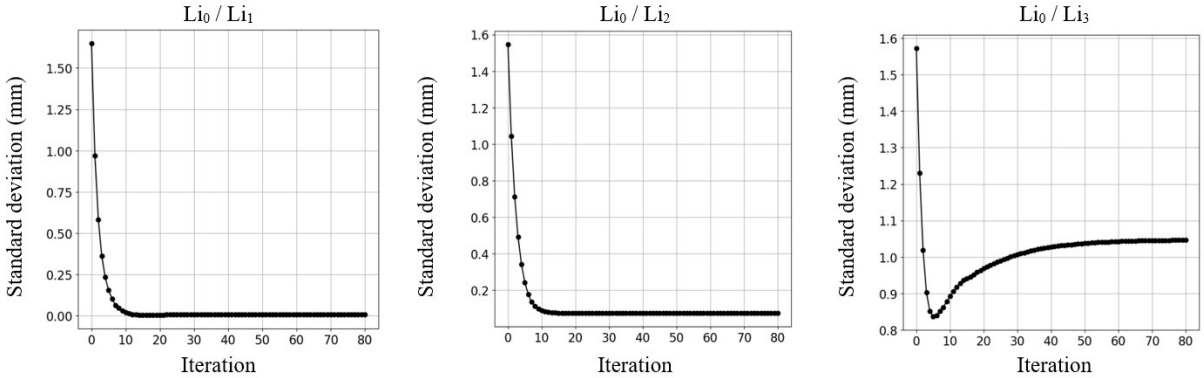

Fig. 17. ICP method applied to corroded links. Standard deviation of distances for Li_1, Li_2 and Li_3 with R_y=3° and T_x=2 mm.

3.2.3. Discussion of the ICP method

The results concerning the uncorroded links show that convergence is regular; the standard deviation is strictly decreasing; it reaches the minimum threshold in all three cases before the maximum number of iterations is exceeded. The maximum error after registration is less than one hundredth of a millimetre for all links, which was expected by setting a standard deviation to be reached of three micrometres. The average of the distances converges quickly after about ten iterations to a value close to that expected at the end of convergence. These results are representative of the numerous calculations carried out with the implementation of the ICP method; they confirm that this method achieves good convergence for links without a reduction in thickness (not corroded).

The results concerning corroded links are different. They show that convergence is not reached; the standard deviation tends towards a value that is too high. The maximum error after registration is high with respect to the corrosion thicknesses t_{hk}. However, as for the uncorroded links, the average distance converges quickly after about ten iterations to a value close to the expected one. These results show that a conventional registration method, of the ICP type, is not suitable for corroded links.

3.3. Iterative method adapted for parts with generalised corrosion (GC-ICP)

Let S_p be the surface of a non-corroded part. Let S_q be the surface of this same part after corrosion. The hypothesis of generalised corrosion implies that the material loss on S_p is identical whatever the point P_i considered. This is a material thickness reduction of t_{hk} mm, in the direction $\vec{n}(P_i)$, normal to S_p at point P_i. The objective of a registration between S_p and S_q is to find the rigid transformation $\mathcal{T}$ such that the distances between S_p and $\mathcal{T}(S_q)$ are all equal to t_{hk}. This objective can be translated by the condition (20).

$$\forall\, Q \in S_q, d\left(S_p, \mathcal{T}(\mathrm{Q})\right) = t_{hk} \tag{20}$$

Unlike a conventional ICP method as implemented previously, it is notable that the target points Pt_i are not located on S_p because the surfaces are shifted by t_{hk} after registration, and not superimposed (see Fig. 18). In the case of major corrosion, it is therefore totally inappropriate to try to approach these target points by the points closest to Q_i on S_p as occurs in the implementation of the ICP method. This explains the poor results previously obtained. The resolution strategy must therefore be modified.

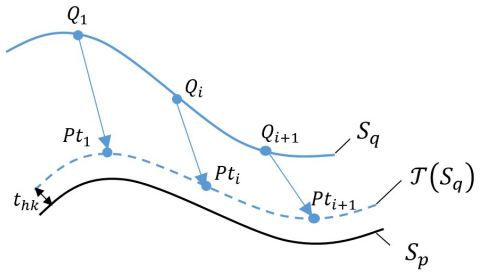

Fig. 18. *Corroded surface S_q with target points after registration.*

In order to resolve the problem, it is proposed here to construct from S_q a surface S'_q with a thickness increased by an *a priori* unknown value t_{hk}. Each point Q_i is thus translated by a distance t_{hk} along $\vec{n}(Q_i)$, the normal to S_q at Q_i (see Fig. 19). Thus, to align S_q onto S_p, it is now sufficient to register S'_q onto S_p by checking condition (21). Since the new target points Pt'_i are now located on S_p, it is possible to once again consider approaching them by the nearest points $H(Q'_i)$.

$$\forall\, Q' \in S'_q, d\left(S_p, \mathcal{T}(\mathrm{Q}')\right) = 0 \tag{21}$$

Note that instead of increasing the thickness of S_q along $\vec{n}(Q_i)$, it is possible to decrease the thickness of S_p along $\vec{n}(P_i)$. Therefore, it is assumed that a point of S_p corrodes along a direction that remains constant with time.

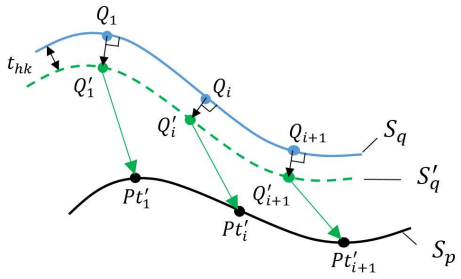

Fig. 19. *Thickness increase then ICP*

At each iteration k, the objective is now to find the transformation $\mathcal{T}_k$ that minimises the objective function g'_k defined by the expression (22), and in vector form by the expression (23).

$$g'_k(S_p, Ec_{q,k-1}) = g_k\left(S_p, Ec'_{q,k-1}\right) = \sum_{i=1}^{N} \left[d\left(Pt'_i, \mathcal{T}_k(Q'_{i,k-1})\right)\right]^2, Q'_{i,k-1} \in Ec'_{q,k-1} \tag{22}$$

$$g'_k(S_p, Ec_{q,k-1}) = \sum_{i=1}^{N} \left[\left\|\overrightarrow{pt'_i} - T_k \cdot \left(\vec{q}_{i,k-1} + t_{hk} \cdot \vec{n}(Q_{i,k-1})\right)\right\|\right]^2, \mathrm{Q}_{i,k-1} \in Ec_{q,k-1} \tag{23}$$

At each iteration, to identify the transformation that minimises g'_k, the points Pt'_i will be approximated by the points $H(Q'_i)$, the closest points to Q'_i on S_p, and the thickness t_{hk} will be estimated by the average of the distances between S_p and S_q at the previous iteration, with this value converging rapidly from the first few iterations. In the iterative process, t_{hk} will not be recalculated at each iteration, but after a certain number of iterations so that the target points Pt'_i do not constantly change. A value equal to fifteen iterations was chosen per experiment.

3.3.1.GC-ICP method tests

The tests performed on corroded links are identical to those defined in 3.2.2. The results of these tests are summarised in Table 6, Fig. 20 and Fig. 21.

Table 6 – GC-ICP applied to corroded links

Fixed link	Moved link	R_y (degree)	T_x (mm)	Mean (mm)	Standard deviation (mm)	Maximum error (mm)	Number of iterations	Calculation time (s)
Li_0	Li_1	3	2	0.0489	0.0028	0.0077	43	395
Li_0	Li_1	6	5	0.0488	0.0028	0.0073	34	254
Li_0	Li_2	3	2	0.4990	0.0029	0.0074	38	299
Li_0	Li_2	6	5	0.499	0.0025	0.0070	22	126
Li_0	Li_3	3	2	4.998	0.0026	0.0070	72	693
Li_0	Li_3	6	5	4.998	0.0022	0.0067	78	731

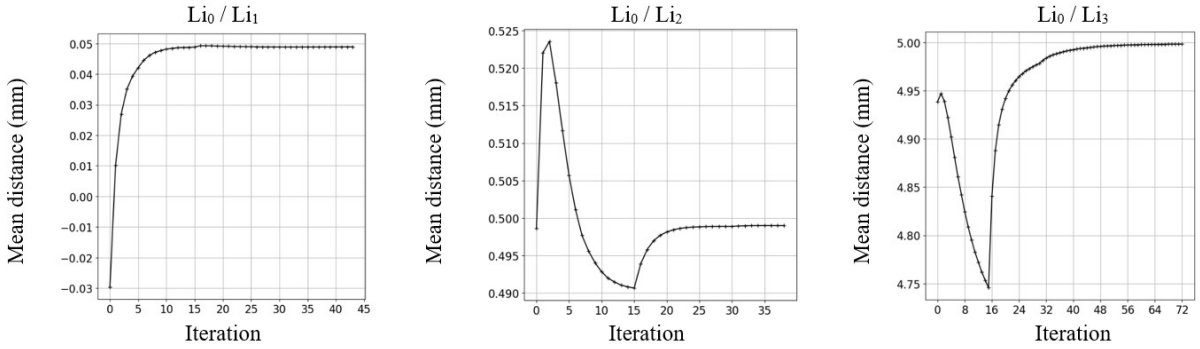

Fig. 20. *GC-ICP method applied to CAD corroded links. Average of distances for Li_1, Li_2 and Li_3 with R_y=3° and T_x=2 mm.*

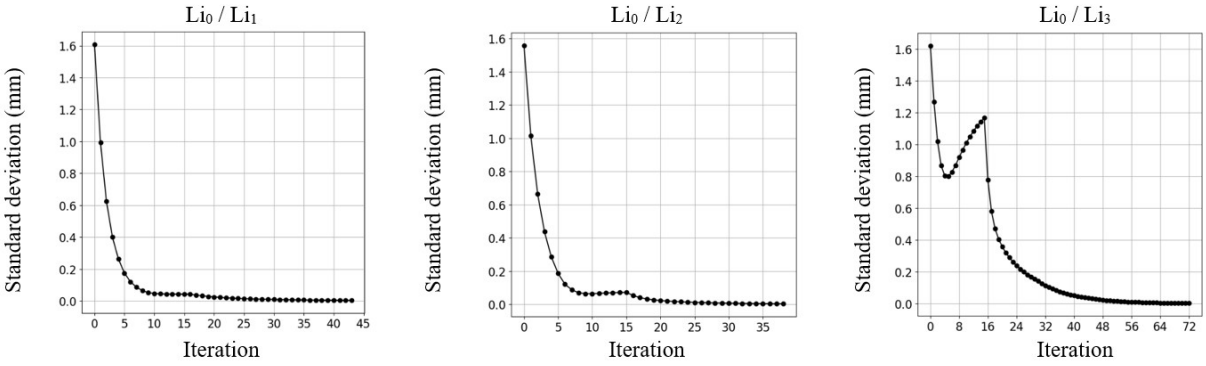

Fig. 21. *GC-ICP method applied to CAD corroded links. Standard deviation of distances for Li_1, Li_2 and Li_3 with R_y=3° and T_x=2 mm.*

3.3.2. Discussion of the GC-ICP method

During the first fifteen iterations, the loss of material being assumed to be zero when minimising g'_k, there is an initial non-convergence of the process. However, during this phase, the average of the distances quickly tends towards a value close to the expected thickness decrease. Every fifteen iterations, t_{hk} is updated by the mean value

of the distances, resulting in discontinuities C^1 of the mean and standard deviation, but the overall process converges to the expected solution. The standard deviation reaches the minimum threshold in all three cases before the maximum number of iterations is exceeded. The maximum error after registration is less than one hundredth of a millimetre for all links. These results are representative of the numerous calculations performed with the implementation of the GC-ICP method; they confirm the good convergence of this method for CAD links with thickness reduction (corroded). However, no test case could be performed on real scans, because it is difficult to obtain standard parts that correspond to the case of material loss encountered. Note that for CAD links, no point is rejected by the distance calculations, as the surface is sufficiently regular for the construction of local smoothing. In the case of real links, a number of points are necessarily rejected (see 2.2.1) and the construction of the smoothings induces inaccuracies in the calculation of the normals. However, the method seems sufficiently robust for several reasons:

- The registration is applied to meshes that have been filtered at the time of their construction. They are therefore little affected by the presence of outliers.
- The calculation of the normals is performed on the smoothing curve and this curve is constructed locally from the first m closest points. If there is an outlier, its influence is compensated by the presence of $m-1$ other points.
- If the local surface does not allow regular smoothing, the point considered on S_q is rejected and therefore is not included in the registration process. In addition to outliers, these points may be local surface discontinuities related to possible pitting corrosion, the presence of residual biological material or other wears and manufacturing defects.

4. Registration for worn and corroded parts

4.1. Focus of the problem

The material losses considered in this work are generalized corrosion losses and localized losses due for example to wear, pitting corrosion or corrosion under the attachment zones of marine organisms, such as barnacles. Thicknesses of localized material losses taken into account are greater than the thickness of generalized corrosion. Consequently, in an alignment process, the distances measured in the locally altered areas are greater than those measured on the rest of the mesh which is only subject to generalized corrosion. Under these conditions, it is not beneficial to perform a standard registration, as these larger distances would necessarily affect the calculation of

the objective function and result in a low accuracy after registration. A new method that takes into account both localized wear and generalized corrosion must therefore be developed.

4.2. Description of the WGC-ICP method

For this new method, it is envisioned that the points in the S_q sample that would be identified as points present on localized areas of material loss, would be filtered out. The links would then be registered on this new reduced sample. After applying the filter, the remaining number of points should be sufficient to ensure that the process achieves good convergence. This method is therefore suitable if the locally altered surface remains limited with respect to the total area of the link analysed. Let Ec_q^w be the point sample of Pc_q that does not feature points present on localized areas of material loss. The objective of registration between S_p and S_q is now to find the rigid transformation $\mathcal{T}$ such that the distances between S_p and $\mathcal{T}\left(Ec_q^w\right)$ are equal to t_{hk} This objective, which can be translated by condition (24), is solved in the same way as the GC-ICP method, but for the filtered sample of points.

$$\forall\, Q_i \in Ec_q^w, d\left(S_p, \mathcal{T}(\mathrm{Q}_i)\right) = t_{hk} \tag{24}$$

Let $D\left(S_p, Ec_q\right)$ be the set of computed distances between the sample points Ec_q of S_q, with the surface S_p. Among these distances, those corresponding to the points present on localized areas of material loss are sparse observations and far from the typical magnitudes of the set of calculated distances. The points of S_q will therefore be considered as local alteration points if their distance from S_p is greater than a cut-off distance d_c to be determined. Fig. 22 presents a typical histogram of the distances $D\left(S_p, Ec_q\right)$ in which one can observe a peak centered on the corrosion thickness and a set of significant distances that correspond to the contact-worn points. Considering that the values below the generalised corrosion thickness are data unaffected by contact wear, the expected dispersion without these cases of contact wear can therefore be estimated, during the iterative process, by symmetrising these distances with respect to the corrosion thickness. The cut-off distance d_c can therefore be calculated as follows:

- Computation of the median on the basis of $D\left(S_p, Ec_q\right) : med\left[D\left(S_p, Ec_q\right)\right]$.
- Removal of points above the median.

- Construction of $D'(S_p, Ec_q)$, the set of distances obtained by symmetrising the distances below the median, with respect to the median.
- Computation of the median absolute deviation on $D'(S_p, Ec_q)$: $mad[D'(S_p, Ec_q)]$.
- Calculation of the cut-off distance d_c defined as a function of a threshold thr and by the relation (25).

$$d_c = med[D(S_p, Ec_q)] + thr \times mad[D'(S_p, Ec_q)] \tag{25}$$

In the proposed method, the median med and the median absolute deviation mad are used in place of the mean and standard deviation to estimate a statistically robust cut-off distance (Hoaglin et al., 2010; Leys et al., 2013), independent of atypical distances. The median absolute deviation mad is defined by the relation (26), in which the k_{dist} value is taken to be 1.4826 in order to make this estimator equivalent to the use of the standard deviation for a normal distribution (Rousseeuw and Croux, 1993). Therefore, the threshold thr chosen is conventionally between 2.5 and 3 depending on the percentage of points to be filtered on $D'(S_p, Ec_q)$.

$$mad[D'(S_p, Ec_q)] = k_{dist} \times med_i(|d_i - med[D'(S_p, Ec_q)]|),\ d_i \in D'(S_p, Ec_q) \tag{26}$$

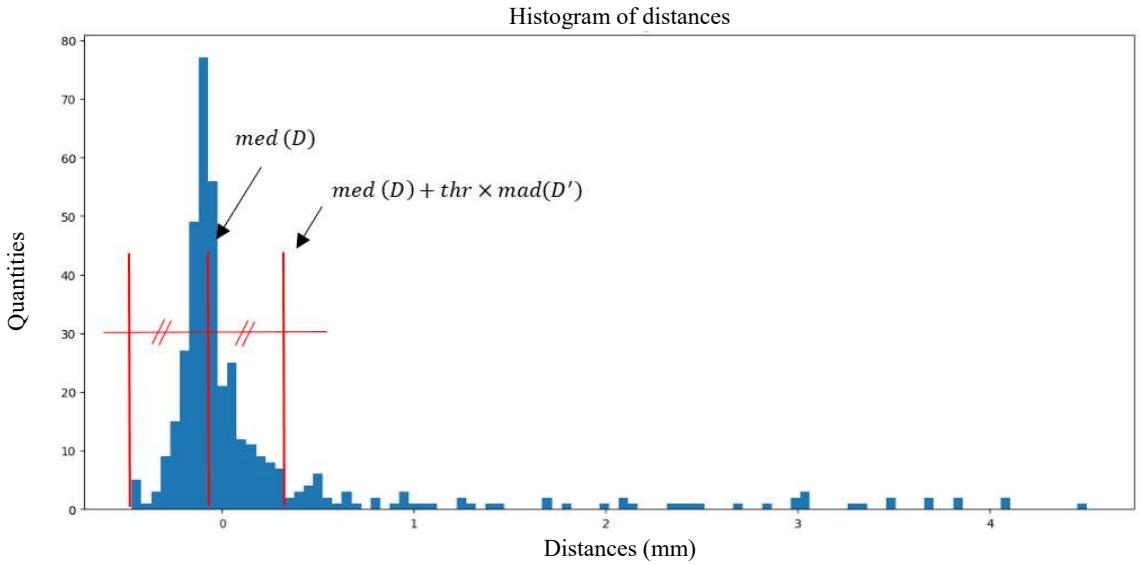

Fig. 22. *Typical histogram of the distances between an aged link and a new link.*

4.3. WGC-ICP method tests

Four links are used to test the implementation of the WGC-ICP method. These are the CAD links Li_6, Li_7, Li_8 and Li_9 described in Table 7. The Li_7, Li_8, Li_9 links are derived from the Li_6 link of the 40-5-3.4 type (see Fig.

23) after reducing material thickness t_{hk} by 3 mm and, respectively, after adding of regular wear in the bends , wear in the form of grooves in the bends, and regular wear with a presence of scattered cavities. The worn links are displaced through space by means of two geometric transformations: $(R_y, T_x) = (-3°, 2\ mm)$ or $(R_y, T_x) = (2°, 4\ mm)$. At the end of the registration process between the altered links and the Li_6 link, and following the removal of points present on localized areas of material loss, the expected distances between links are equal to the corrosion thickness. The results of these calculations are summarised in Table 8, in Fig. 24 and Fig. 25. The parameterisation of the registrations is identical to that defined in section 3.2.1.2. After the first 15 fast-approach iterations, the generalised corrosion thickness calculation and the points filter are updated every 10 iterations. The value of the thr threshold is set to 3.

***Table 7** - Characteristics of links*

Links	b_s (mm)	t_{hk} (mm)	n_p	File size (Mo)
Li_6	0.28	0	1 750 140	171
Li_7	0.44	3	1 487 642	145
Li_8	0.33	3	2 458 041	240
Li_9	0.33	3	2 758 610	269

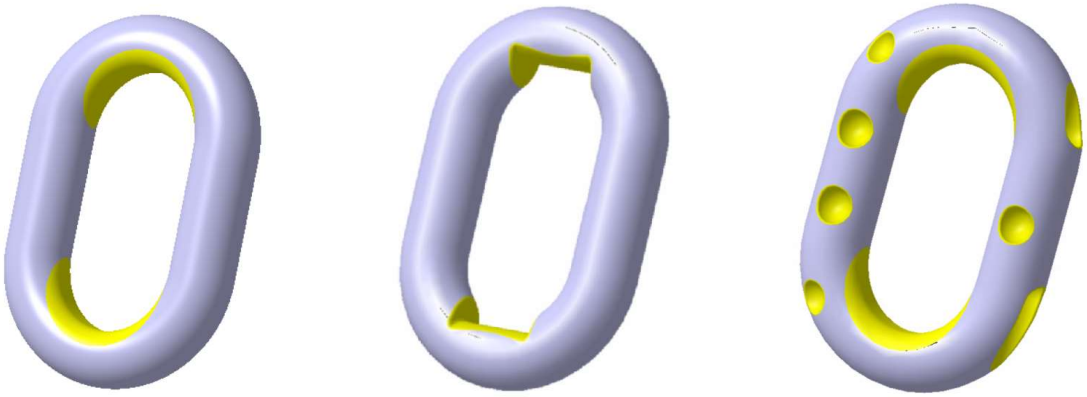

(a) (b) (c)

***Fig. 23.** Local decreases in thickness are shown in yellow. (a) Link Li_7. (b) Link Li_8. (c) Link Li_9.*

***Table 8** – WGC-ICP applied to links with generalised corrosion and localised alterations*

Fixed link	Moved link	R_y (degree)	T_x (mm)	Mean (mm)	Standard deviation (mm)	Maximum error (mm)	Number of iterations	Calculation time (s)

Li_6	Li_7	-3	2	2.9999	0.0028	0.0074	68	1008
Li_6	Li_7	2	4	2.9989	0.0028	0.0075	81	1181
Li_6	Li_8	-3	2	2.9988	0.0025	0.0085	64	948
Li_6	Li_8	2	4	2.9989	0.0029	0.0074	49	725
Li_6	Li_9	-3	2	2.9993	0.0025	0.0113	81	1205
Li_6	Li_9	2	4	2.9992	0.0036	0.0096	120	1921

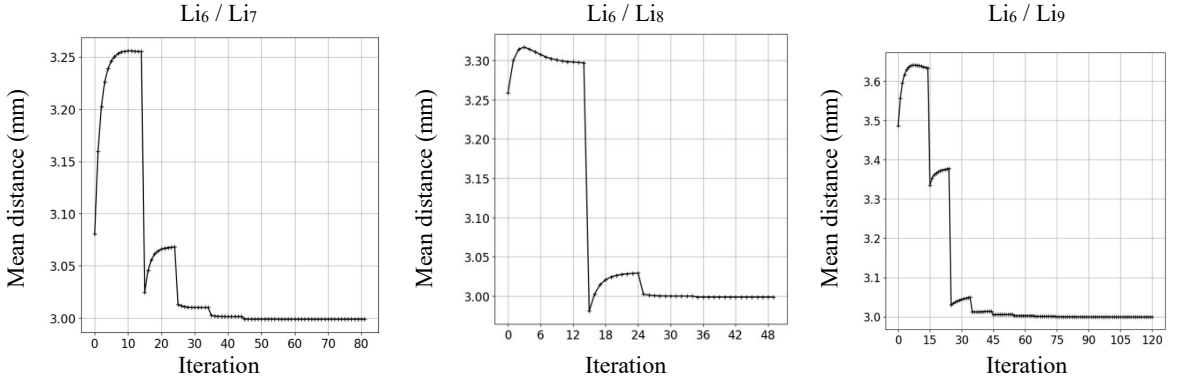

Fig. 24. WGC-ICP method applied to links with generalised corrosion and localised alterations. Mean distances for Li_7, Li_8 and Li_9 with Ry=2° and Tx=4 mm.

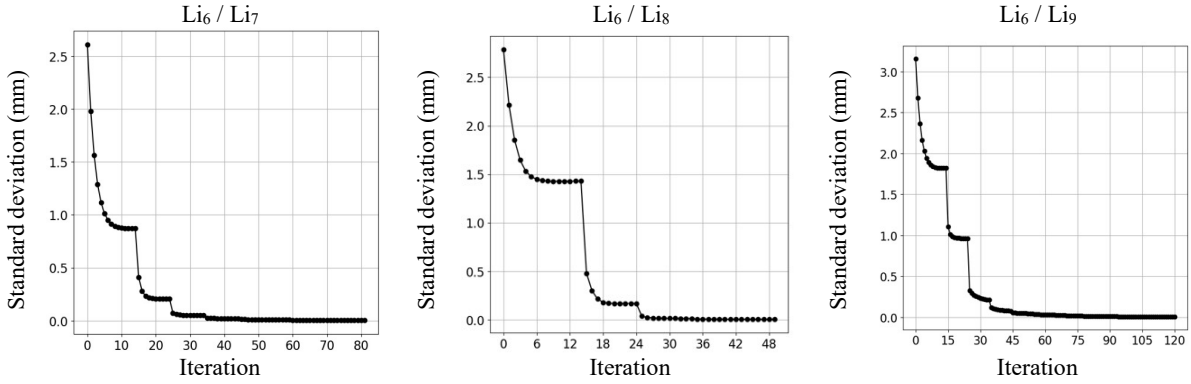

Fig. 25. WGC-ICP method applied to links with generalised corrosion and localised alterations. Standard deviation of distances for Li_7, Li_8 and Li_9 with R_y=2° and T_x=4 mm.

4.4. Discussion of the WGC-ICP method

Every ten iterations, t_{hk} is updated by averaging the distances and the points present on the localized material loss areas are filtered. This results in C^1 discontinuities in the mean and standard deviation, but the process converges to the expected solution. It is noticeable that the filter is only applied to a sample of points $Ec_q$of S_q, it is not intended to accurately identify all the points affected by localised material loss. The goal here is to remove the points that may have a negative influence on the link alignment process. The maximum error obtained after registration is close to one hundredth of a millimetre for all the tested links. However, the number of required

iterations and the computation time are significantly higher than with previous methods. These results are representative of the numerous calculations carried out with the implementation of the WGC-ICP method, they confirm that this method achieves good convergence for CAD links. For illustration purposes, Fig. 26 shows the points identified by the algorithm as being located on areas of localised material loss for the Li_9 link. On Fig. 26(b) and in Fig. 26(c) sections of the same link are represented, superimposed with the unaltered mesh, and this before and after the registration process.

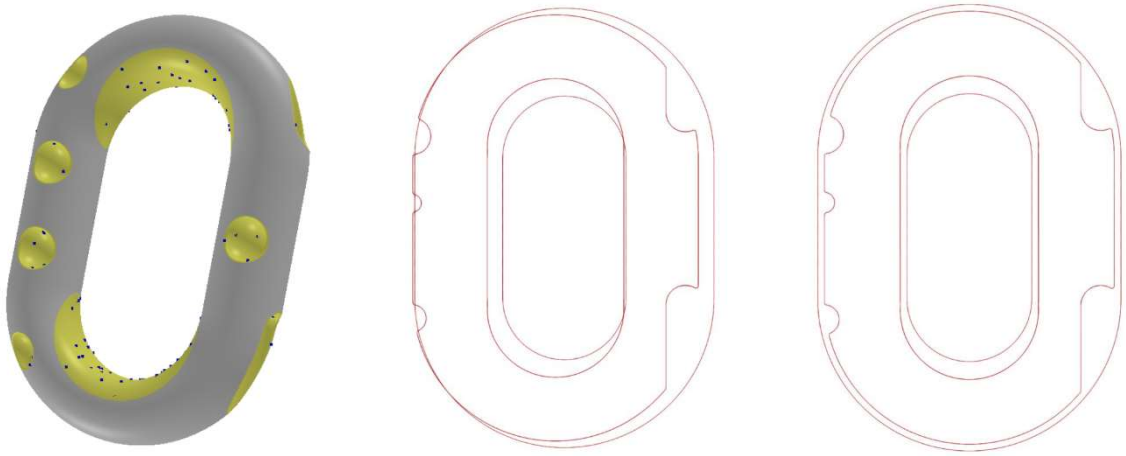

Fig. 26. *(a) The points identified by the WGC-ICP filter are shown in blue on the Li9 link. (b) Cross-section of the Li6 and Li9 links overlay before registration, (c) Cross-section of the Li6 and Li9 links overlay after registration.*

In the process of removing the points present on the localized material loss areas, it may be necessary to check that the remaining points are associated with normals with directions in space that do not have a preferred perpendicular axis. For example, the remaining points after a filter on a link with wear on both the inside and the outside of the bends would possess normals that are mainly perpendicular to the $(O, \vec{x})$ axis. Under these conditions, it would be difficult to find a precise position in this direction.

5. Conclusions

In order to improve knowledge of the ageing of mooring chains, it may be necessary to carry out temporal monitoring of material losses to better understand their kinetics and origins. For example, this can be done by periodically identifying changes in the 3D geometry of chain links immersed at sea, or artificially altered in laboratory. The use of 3D scanners allows these geometries to be captured and then compared after superposition. However, this superposition is not trivial because in most cases the entire surface of the link is altered during ageing, and because the acquisition process produces data written in different reference frames. A specific

alignment algorithm adapted to the encountered ageing problem is proposed in the present work. The results which are obtained allow us to present the following conclusions.

- It is necessary to perform local smoothing operations on the scan meshes to evaluate the distances, before considering an accurate alignment process. This is because a conventional distance calculation method, of the point-to-point type, does not provide sufficient accuracy when the expected distances are of the order of magnitude of the facet edges of the meshes. A point-to-curve calculation method has therefore been developed. It is based on local polynomial smoothing, controlled by acceptability criteria. This proposed method provides: an accurate distance calculation (2.2.2), an estimation of the nearest point normal, and an outlier filter.
- The conventional ICP registration methods cannot be applied in the presence of generalised corrosion, because the approximation of the target point by means of the nearest point is inadequate when the corrosion thickness becomes significant (3.2.2.2). These methods are also sensitive to the presence of outliers, which in the case studied are mainly the points present on the localized material loss areas.
- The GC-ICP method developed proposes building an extra-thick section of material onto one of the meshes, the thickness of which is defined after a few iterations by the average of the distances between an aged link and a new link. The convergence obtained with the modified mesh is regular and the accuracy achieved with the chosen parameterisation is lower than a hundredth of a millimetre (3.3.2) for CAD-type links.
- The WGC-ICP method developed eliminated the points present on the localized alterations from the registration process by using a statistically robust filter. Insofar as we consider that these alterations remain limited in relation to the total surface of the analysed link, the removal of the points has little effect on the registration process and the results converge, for CAD links, to errors that are just as low as those of the GC-ICP method (4.3). This alignment method is adapted to the geometrical specificities of mooring chain links that have been in the marine environment or any other mechanical part subject to the same type of physico-chemical aggression. It allows to consider a three-dimensional, temporal and precise geometrical monitoring of the material losses.

The present conclusions regarding the developed registration methods are based on numerical tests using perfect meshes from CAD constructions representing typical geometries of mooring chain links that have been in the

marine environment. Future work can now be considered to test the robustness of these methods on meshes from scans of real mechanical parts with the same specificities.

Authors contributions

Y. Argouarc'h : Funding acquisition, Project administration, Conceptualisation, Methodology, Software, Data curation, Validation, Writing - original draft, Writing - review & editing, Visualisation.

R. Creac'hcadec : Funding acquisition, Project administration, Methodology, Writing - review & editing, Visualisation.

Declaration of competing interest

The authors declare that they have no known competing financial interests or personal relationships that could have influenced the work reported in this article.

Acknowledgements

The authors are grateful to the Technical Department for water, sea and rivers (Brest, France) of CEREMA, the French centre for studies and expertise concerning risks, the environment, transport and land use planning for its contribution to financing the project on the study of the wear of anchor chains exposed to the marine environment. In particular, the authors would like to thank Mr Philippe Renaudin, an expert in mooring lines, for his experience and support. The authors would also like to thank Mr. Guillaume Sicot (UMR CNRS 6285, Lab-STICC, ENSTA Bretagne / HOP, F-29200 Brest, France) for his sound advice and Mr Thibault Maillard for his contribution to the first works on this project.

Bibliography

Artec studio professional 15, 2020. Artec Europe.

Arun, K.S., Huang, T.S., Blostein, S.D., 1987. Least-Squares Fitting of Two 3-D Point Sets. IEEE Transactions on Pattern Analysis and Machine Intelligence PAMI-9, 698–700. https://doi.org/10.1109/TPAMI.1987.4767965

Bellekens, B., Spruyt, V., Berkvens, R., Penne, R., Weyn, M., 2015. A Benchmark Survey of Rigid 3D Point Cloud Registration Algorithms 11.

Besl, P.J., McKay, N.D., 1992. A method for registration of 3-D shapes. IEEE Transactions on Pattern Analysis and Machine Intelligence 14, 239–256. https://doi.org/10.1109/34.121791

Bowyer, K.W., Chang, K., Flynn, P., 2006. A survey of approaches and challenges in 3D and multi-modal 3D+2D face recognition. Computer Vision and Image Understanding 101, 1–15. https://doi.org/10.1016/j.cviu.2005.05.005

CEREMA, 1997. Signalisation maritime - Documentation technique - Exploitation du balisage - Lignes de mouillage.

Chen, Y., Medioni, G., 1992. Object modelling by registration of multiple range images. Image and Vision Computing, Range Image Understanding 10, 145–155. https://doi.org/10.1016/0262-8856(92)90066-C
Dawson-Haggerty, M., 2019. Trimesh.
D'Souza, R., Majhi, S., 2013. Application of Lessons Learned From Field Experience to Design, Installation and Maintenance of FPS Moorings. Presented at the Offshore Technology Conference, OnePetro. https://doi.org/10.4043/24181-MS
Eashwar, M., Subramanian, G., Chandrasekaran, P., Balakrishnan, K., 1992. Mechanism for Barnacle-Induced Crevice Corrosion in Stainless Steel. Corrosion 48, 608–612. https://doi.org/10.5006/1.3315979
Fontaine, E., Kilner, A., Carra, C., Washington, D., Ma, K.T., Phadke, A., Laskowski, D., Kusinski, G., 2014. Industry Survey of Past Failures, Pre-emptive Replacements and Reported Degradations for Mooring Systems of Floating Production Units. Presented at the Offshore Technology Conference, OnePetro. https://doi.org/10.4043/25273-MS
Fontana, S., Cattaneo, D., Ballardini, A.L., Vaghi, M., Sorrenti, D.G., 2020. A Benchmark for Point Clouds Registration Algorithms 36.
Gordon, R.B., Brown, M.G., Allen, E.M., 2014. Mooring Integrity Management: A State-of-the-Art Review, in: Day 4 Thu, May 08, 2014. Presented at the Offshore Technology Conference, OTC, Houston, Texas, p. D041S047R006. https://doi.org/10.4043/25134-MS
Hoaglin, D.C., Mosteller, F., Tukey, J.W., 2010. Understanding Robust and Exploratory Data Analysis, New e. édition. ed. Wiley, New York.
Hurley, J.R., Cattell, R.B., 1962. The procrustes program: Producing direct rotation to test a hypothesized factor structure. Behavioral Science 7, 258–262. https://doi.org/10.1002/bs.3830070216
IACS, 2010. Guidelines for the Survey of Offshore mooring Chain Cable in Use.
IALA, 2010. Design of Floating Aid to Navigation Moorings 1066.
Kraft, D., 1988. A software package for sequential quadratic programming.
Leys, C., Ley, C., Klein, O., Bernard, P., Licata, L., 2013. Detecting outliers: Do not use standard deviation around the mean, use absolute deviation around the median. Journal of Experimental Social Psychology 49, 764–766. https://doi.org/10.1016/j.jesp.2013.03.013
Lotfollahi Yaghin, A., Melchers, R.E., 2015. Long-term inter-link wear of model mooring chains. Marine Structures 44. https://doi.org/10.1016/j.marstruc.2015.08.001
Ma, K., Shu, H., Smedley, P., L'Hostis, D., Duggal, A., 2013. A Historical Review on Integrity Issues of Permanent Mooring Systems. Presented at the Offshore Technology Conference, OnePetro. https://doi.org/10.4043/24025-MS
Maneewongvatana, S., Mount, D.M., 1999. Analysis of approximate nearest neighbor searching with clustered point sets. arXiv:cs/9901013.
Murugan, V.K., Mohanram, H., Budanovic, M., Latchou, A., Webster, R.D., Miserez, A., Seita, M., 2020. Accelerated corrosion of marine-grade steel by a redox-active, cysteine-rich barnacle cement protein. npj Mater Degrad 4, 20. https://doi.org/10.1038/s41529-020-0124-z
Pomerleau, F., Colas, F., Siegwart, R., 2015. A Review of Point Cloud Registration Algorithms for Mobile Robotics. FNT in Robotics 4, 1–104. https://doi.org/10.1561/2300000035
Potts, A., Kurts, P., Jayasinghe, K., Kilner, A., Melchers, R., Lee, T., Chaplin, R., 2018. SCORCH JIP - Overview of Project and Summary of Findings, in: Day 3 Wed, May 02, 2018. Presented at the Offshore Technology Conference, OTC, Houston, Texas, USA, p. D032S092R002. https://doi.org/10.4043/29017-MS
Rousseeuw, P.J., Croux, C., 1993. Alternatives to the Median Absolute Deviation. Journal of the American Statistical Association 88, 1273–1283. https://doi.org/10.1080/01621459.1993.10476408
Scipy spatial KDTree [WWW Document], 2011. URL https://docs.scipy.org/doc/scipy/reference/generated/scipy.spatial.KDTree.html (accessed 4.30.21).
Sorkine-Hornung, O., Rabinovich, M., 2017. Least-Squares Rigid Motion Using SVD 5.
Turk, G., Levoy, M., 1994. Zippered polygon meshes from range images, in: Proceedings of the 21st Annual Conference on Computer Graphics and Interactive Techniques - SIGGRAPH '94.

Presented at the the 21st annual conference, ACM Press, Not Known, pp. 311–318. https://doi.org/10.1145/192161.192241

Yambor, W.S., Draper, B.A., Beveridge, J.R., 2002. Analyzing PCA-based Face Recognition Algorithms: Eigenvector Selection and Distance Measures, in: Series in Machine Perception and Artificial Intelligence. WORLD SCIENTIFIC, pp. 39–60. https://doi.org/10.1142/9789812777423_0003